

Kai Frings · Rüdiger Lutz · Helga de Wall ·  
Laurence N. Warr

## Coalification history of the Stephanian Ciñera-Matallana pull-apart basin, NW Spain: Combining anisotropy of vitrinite reflectance and thermal modelling

Received: 30 January 2003 / Accepted: 1 November 2003 / Published online: 16 January 2004  
© Springer-Verlag 2004

**Abstract** The Stephanian Ciñera-Matallana Basin of NW Spain comprises 1,500 m of alluvial to lacustrine coal-bearing sediments, which were deposited in a late Variscan transtensional/transpressional pull-apart setting. The relationship between coalification pattern and rock deformation was evaluated by measurements of the anisotropy of vitrinite reflectance (AVR). The AVR ellipsoids reveal both pre-tectonic elements related to the bedding fabric and syn-tectonic elements related to folding, producing biaxial ellipsoid shapes with the maximum reflectance parallel to fold axes. The mean coalification gradient for the Stephanian succession is about 0.62 %Rr/km. Calculations of the mean palaeo-geothermal gradient are presented on the basis of three different empirical equations. A palaeo-geothermal gradient of 85 °C/km is considered the most realistic, with an overburden of about 1,000 m. 1-D numerical modelling of the burial history results in two possible scenarios, the most preferable involving a palaeo-heat flow of 150 mW/m<sup>2</sup> and an overburden of ca. 1,050 m. These results indicate that maximum coalification was related to a localised but high palaeo-heat flow/-geothermal gradient. The anisotropy of vitrinite reflectance highlights the interactive and transitional nature of sedimentary compaction and rock deformation on the maturation of organic material within strike-slip fault zones.

**Keywords** Ciñera-Matallana · Coalification · Palaeo-geothermal gradient · Palaeo-heat flow · Anisotropy of vitrinite reflectance

### Introduction

The Stephanian Ciñera-Matallana Basin (CMB), located in the Cantabrian Zone of NW Spain (Fig. 1A), is one of the most important coal mining districts of the Iberian Peninsula with more than 100 years of mining tradition. Despite this, no published study has attempted a quantitative characterisation of the overall coalification and thermal history of this small, fault-related pull-apart basin. The CMB is one of several Stephanian coal basins positioned along the southern border of the Cantabrian Zone, all of which have complex depositional and tectonic histories. These strike-slip fault related basins, especially the CMB, are positioned in key sites for unravelling the geological and thermal development of the Cantabrian Zone during the late stages of the Variscan orogeny (García-Lopez et al. 1999), and the transition to Permian crustal extension and volcanism (Fernandez-Suarez et al. 2000).

There is a long tradition in using the patterns of coalification to reconstruct the thermal history of sedimentary basins (Teichmüller 1987a; Yalcin et al. 1997; Taylor et al. 1998, and references herein). The distribution of coalification grade, measured by the random vitrinite reflectance (%Rr), enables construction of surface maps and cross sections that incorporate isoreflectance lines (e.g. Kalkreuth et al. 1989; Hertle and Littke 2000). The geometric relationship between isoreflectance lines and bedding planes allows differentiation between pre-, syn- and post-tectonic coalification at a regional scale (Teichmüller and Teichmüller 1966). To evaluate the relationship between coalification and tectonic deformation in greater detail, the anisotropy of vitrinite reflectance (AVR) can also be measured. During the process of coalification the inner aromatic structure of the organic material responds to directional stress

---

K. Frings (✉) · L. N. Warr  
Geologisch-Paläontologisches Institut,  
Ruprecht-Karls-Universität,  
Im Neuenheimer Feld 234, 69120 Heidelberg, Germany  
e-mail: kai.frings@gmx.net  
Fax: +49-06221-545503

R. Lutz  
Bundesanstalt für Geowissenschaften und Rohstoffe BGR,  
Stilleweg 2, 30655 Hannover, Germany

H. de Wall  
Institut für Geologie,  
Bayerische Julius-Maximilians Universität,  
Pleicherwall 1, 97070 Würzburg, Germany

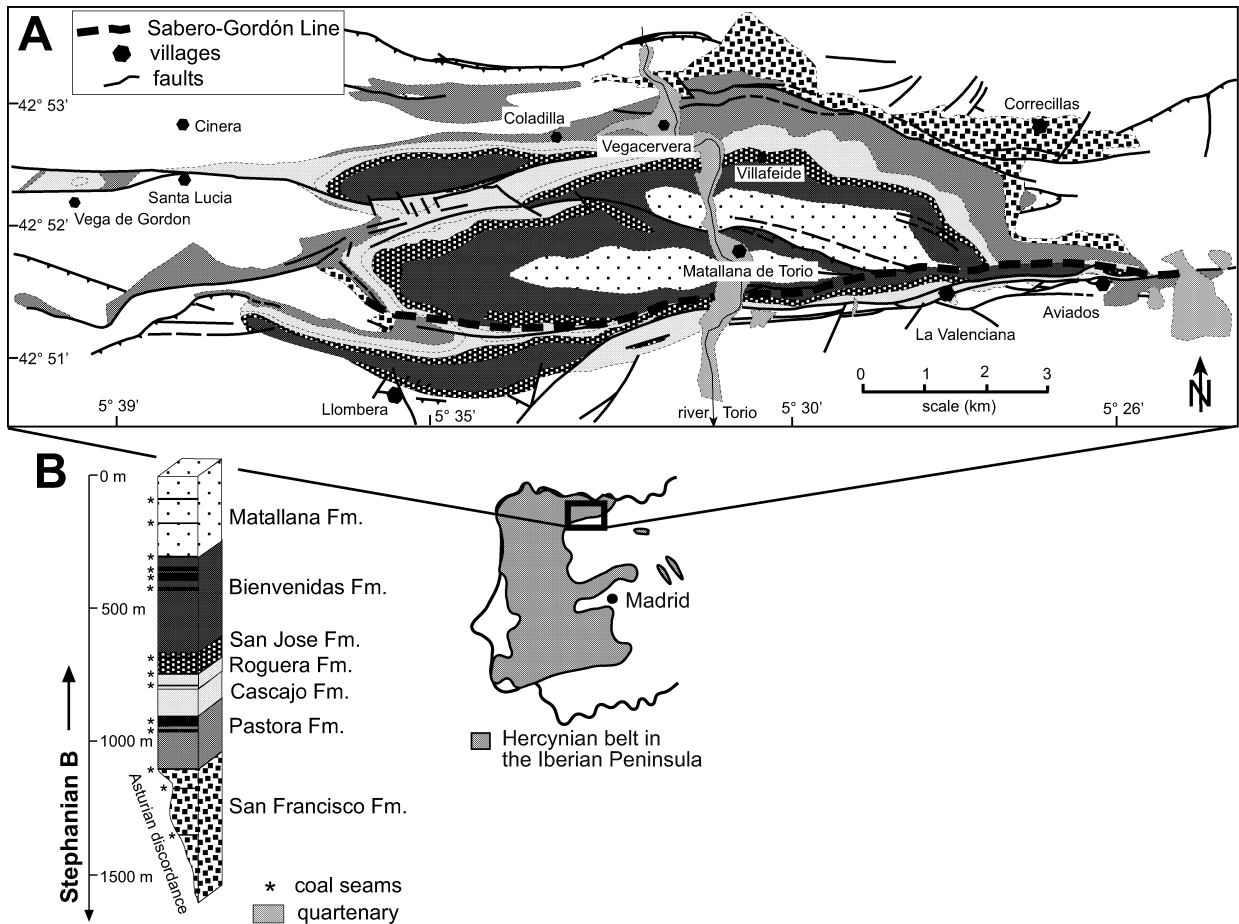


**Fig. 1** A Geological map of the Ciñera-Matallana coal basin. The late orogenic pull-apart basin shows a complex tectonic structure related to strike-slip movements along the Sabero-Gordón line (E–W direction) and mostly compressional deformation (N–S direc-

tion). It is subdivided into several faulted synclines and anticlines. B Sedimentary sequence showing the maximum thickness of the coal-bearing formations within the basin, which rest unconformably on surrounding Lower Palaeozoic units

regimes, such as those induced during compaction and/or tectonic deformation (Hirsch 1954; Levine and Davis 1984, 1989; Teichmüller 1987a; Rouzaud and Oberlin 1990). The orientation of the optical anisotropy can be compared with the geometry of deformation structures. Determination of the AVR from carefully constrained field structures (e.g. folds and faults) enables the timing of coalification to be assessed in relation to strain history, i.e. pre-, syn- and post-stages of maturation (e.g. Stone and Cook 1979; Ting 1981; Hower and Davis 1981a, 1981b; Levine and Davis 1984, 1989; Langenberg and Kalkreuth 1991a, 1991b; Langenberg et al. 1998; Gibbling et al. 2002). Such knowledge provides useful constraints for improving the thermal modelling of sedimentary basins.

Based on %Rr-data, the construction of isoreflectance lines is commonly used to estimate coalification gradients for stratigraphic successions dominated by burial diagenesis. In such cases isoreflectance lines should run parallel or sub-parallel to bedding (Yamaji 1986). Palaeo-geothermal gradients can be determined by converting the %Rr data into temperature values. Several

empirical equations and methods have been presented, based on various assumptions and correlations, each with varying emphasis on the importance of time and temperature during the coalification process (Lopatin 1971; Waples 1980; Barker and Pawlewicz 1986, 1994; Barker and Goldstein 1990; Sweeney and Burnham 1990; Mullis et al. 2001). For discussion of some of the most frequently used procedures, the reader is referred to Sachsenhofer and Littke (1992). Calculation of palaeo-geothermal gradients and knowledge of the maximum coalification also allows estimation of the thickness of eroded overburden.

Another approach to study the thermal history of sedimentary basins is by numerical modelling of palaeo-heat flow and burial history, which has proved an essential tool for petroleum exploration (Welte et al. 1997). The modelling procedure typically starts with a conceptual model, based on the recognised geological processes such as deposition, non-deposition, and erosion (Welte and Yalcin 1988). The validity of such models depends on the quality of the input data, which incorporates, for example, the exact stratigraphical thickness and

thermal conductivity of individual layers (Nöth et al. 2002). By far the most widely used data for calibration of these models are measurements of the random vitrinite reflectance (%Rr), which can be compared with modelled reflectance values, such as those calculated by the kinetic EASY %Ro-method of Sweeney and Burnham (1990).

In the study presented, we combine and apply the various approaches for characterising and modelling the thermal history to a small, pull-apart Upper Carboniferous basin of the CMB, NW Spain. This coal-bearing succession offers an ideal chance to investigate the coalification history of a basin, in which sedimentation, rock deformation, and magmatic intrusion were intimately related to late Variscan strike-slip fault activity. Emphasis is given to establishing the timing of coalification in relation to basin evolution and to a quantitative evaluation of the thermal history.

### Geological setting and previous studies

The CMB is located at the southern border of the Cantabrian Mountains in NW Spain (Fig. 1A). The small, intramontane basin (25 km<sup>2</sup>) developed as a fault-related, pull-apart during the late stages of the Variscan orogeny. It forms one of a series of post-Asturian synclinoria that follow the arcuate strike of the Cantabrian Zone (Lotze 1945; Julivert 1971). Lying unconformably upon older strata, known as the Asturian discordance, the 1,500 m thick sedimentary sequence of Stephanian B age is subdivided into seven formations (Wagner and Artieda 1970; Wagner 1971) (Fig. 1B). These formations comprise lacustrine and fluvial sand, silt and mudstones and include more than ten productive coal seams. The whole succession is strongly folded and faulted with the development of several large scale synclines that resulted from N–S compressional deformation of either Variscan (Saalic phase) (Wagner and Artieda 1970; de Sitter 1965) and/or Alpine age (Villegas 1996). The geological development of the basin is directly related to transpressional/transensional movements along the E–W trending Sabero-Gordón line, a sinistral strike-slip fault, which marks the southern border of the CMB (Heward and Reading 1980; Nijman and Savage 1989). Magmatic intrusions (295–286 Ma, Fernandez-Suarez 1998) can be found as dykes and folded sills mainly in the Pastora Formation of the basin. Up to now it is not clear whether these intrusions were post-tectonic (Fernandez-Suarez 1998) or already syn-sedimentary. Coal seams acted as preferential paths for the magmatic melt, forming natural coke along intrusive contacts. Due to the extensive open cast mining, the area contains numerous outcrops of varying size and quality.

Published studies concerning the CMB have mainly dealt with clay mineral reactions and the illite crystallinity index as an indicator for low- to very low-metamorphic grades (Galan et al. 1978; Bieg and Burger 1992; Krumm 1992; Marschik 1992; Frings 2002). An anomalous distribution of metamorphic grade ranging from diagen-

esis to the upper anchizone has been recognised in some parts of the basin, with no apparent relation of clay mineral reactions to burial depth (Frings 2002). Galan et al. (1978) estimated maximum temperatures between 150–200 °C during post-Stephanian/pre-Triassic times, pressures of  $\leq 2$  Kb and a palaeo-geothermal gradient of 60 °C/km, assuming a maximum sediment thickness of 2,500 m. In a more recent illite crystallinity study, Frings (2002) estimated maximum temperatures of  $\leq 200$ –250 °C by using the correlation table of Merriman and Kemp (1996).

Details of the geological history of the CMB are contained within two unpublished doctoral theses (Mendez 1985; Villegas 1996). Mendez (1985) adopted the methods of Karweil (1956) and Lopatin (1971) for conversion of %Rr-data into temperatures and estimated palaeo-thermal conditions of 85–95 °C at depths of 500–1,000 m without magmatic influence and 95–122 °C at equivalent depths with magmatic influence. The contact thermal effects of the intrusive material were considered to be only local. The temperature of the initial magma was considered to be 800–850 °C, the contact with coal at about 603–720 °C, and the contact with the pelitic rocks at 507–637 °C. Based on the above considerations, Mendez (1985) defined a palaeo-geothermal gradient of 7–8 °C/100 m for the Stephanian succession, with significant anomalies in the vicinity of intrusive bodies. He also constructed isorefectance lines for the Pastora Fm. in the West of the basin, which hosts most of the intrusive bodies. The coalification was considered to be partly post-folding since the maximum values of vitrinite reflectance occur in the synclines and the minimum values in the anticlines. Villegas (1996) evaluated a new underground mine in the western part of the basin (“Tabliza Mine”), highlighting sedimentological and structural aspects.

### Analytical methods

Random vitrinite reflectance (%Rr) and gradient calibration

A total of 31 seam samples (“channel sampling”) were collected from surface outcrops of the six youngest formations and prepared following the procedure of Taylor et al. (1998). Due to intense weathering of the coal the polishing process was the most difficult stage of preparation. All measurements of vitrinite reflectance (random and anisotropy) were carried out following the international standard ISO 7404/5 in oil immersion (refractive index  $n=1.518$ ) at x500 magnification and in reflected light (wavelength of 546 nm), utilising a Leitz-DM RXP microscope with a MPV control unit and the computer program MEAS (distributed and copyright by Leica in 1998). For calibration, four different standards were used, their reflectance ranging from 0.589% up to 3.225%. Each presented value of %Rr is based on the

**Table 1** Input of the basic geological data for the numerical 1D modelling of the temperature (palaeo-heat flow) and burial history. Model A assumes an eroded thickness of 2,000 m and Model B a thickness of 1,050 m (values printed bold). The vertical thermal

conductivity of each lithology is given at 20 °C and 100 °C. For other temperatures a linear interpolation/extrapolation is performed to calculate the thermal conductivity

Stratigraphy	Depth		Present		Deposition age		Erosion age		Lithology	Thermal conductivity	
	Bottom (m)	Top (m)	Thickness (m)	Erosion (m)	From (Ma)	To (Ma)	From (Ma)	To (Ma)		@20 (°C)	@100 (°C)
Cretaceous	0	0	0	800	140	65	65	0	Siltstone	2.14	2.03
Eroded Paleozoic	0	0	0	<b>A: 2000</b> <b>B: 1050</b>	290	250	250	200	Siltstone	2.14	2.03
Matallana	300	0	300		291	290			Sandstone	3.12	2.64
Bienvénidas	680	300	380		292	291			Sandstone	3.12	2.64
San Jose	770	680	90		293	292			Sand and silt	2.59	2.31
Roguera	840	770	70		294	293			Shale	1.98	1.91
Cascajo	1,010	840	170		295	294			Shale	1.98	1.91
Pastora	1,210	1,010	200		296	295			Sand and silt	2.59	2.31
San Francisco	1,610	1,210	400		297	296			Sand congl	2.93	2.63
Sed Basement1	2,610	1,610	1,000		355	310	303.5	297	Limestone	2.83	2.56
Sed Basement2	3,610	2,610	1,000		400	355	310	303.5	Siltstone	2.14	2.03

arithmetic mean of 100 measurements per sample, recorded in non-polarised light.

Since formations vary greatly in thickness throughout the basin and are complexly faulted, the precise litho-stratigraphical positions of individual samples could not be defined. As a result the arithmetic mean was plotted against the maximum litho-stratigraphical thickness for each relevant formation, based on the thickness estimates given by Wagner (1971), and the calibration data placed in the middle of each formation.

#### Anisotropy of vitrinite reflectance (AVR)

Measurements of the AVR were carried out on 13 oriented mudstones and pelitic siltstones containing dispersed organic material (DOM), selected from well-constrained structural positions around folds exposed in surface outcrops. The analytical procedure followed that of Langenberg and Kalkreuth (1991b), which has the advantage that measurements can be obtained without the necessity to rotate the object stage of the microscope. Each sample was cut into three perpendicular sections and six directions were measured using polarised reflected light (546 nm) in oil immersion. The polariser was fixed to measure the direction parallel to the polarised light. The reflectance values for each direction are based on 50 measurements and the arithmetic mean calculated.

The AVR was determined by mathematically fitting an ellipsoid to the reflectance measurements data from the six directions following the methodology developed by Kelker and Langenberg (1997). The ellipsoid is defined by the amplitude and orientation of its three principal axes (Max, Int, Min), which correspond to the principal reflectance axes ( $R_{\max}$ ,  $R_{\text{int}}$ ,  $R_{\min}$ ). The foliation of the ellipsoid is defined by the plane containing  $R_{\max}$  and  $R_{\text{int}}$ , and the lineation by the orientation of the  $R_{\max}$  axis. The shape of the AVR ellipsoids can be described either as

uniaxial-/biaxial positive or –negative, and as oblate or prolate (Levine and Davis 1989; Flinn 1962).

The measurement errors involved in calculating AVR ellipsoids ranged, on average, between 6.0–12.2%, with errors been generally higher for DOM than coal preparates. For pure coal samples, the AVR is influenced by vertical differential pressure induced by compaction and/or reorientation of the aromatic lamellae during finite tectonic strains. The AVR of DOM in clastic lithologies may also be influenced by surrounding mineral grains, which cause tangential stresses at the rims of vitrinite particles during compaction and/or rock deformation (Teichmüller 1987b; Levine and Davis 1989). The effect of mechanical rotation may be also a contributing factor. As no significant differences in the AVR ellipsoids were observed between measurements made at the Heidelberg and Aachen laboratories on the same samples, variations due to microscope optics are here considered to be negligible.

#### Numerical 1D-modelling

All random vitrinite reflectance data of the outcrop samples were used to construct one idealised pseudo-well. This technique is explained in detail by Oncken (1982) and Nöth et al. (2001). Simulations of palaeo-heat flow and burial history were performed using the 1D *Petromod* modelling software of IES, Jülich (Germany). For calibration, the kinetic EASY %Ro approach of Sweeney and Burnham (1990) was applied. Modelling was performed by varying the palaeo-heat flow until a best fit was attained between measured and calculated %Rr data (calibration procedure). The input data is presented in Table 1.

For simplicity, the folded basement beneath the Asturian discordance was assumed to be Westphalian limestone of the Valdeteja Formation and Westphalian siltstone of the San Emiliano Formation, which are the

most abundant lithologies underlying and surrounding the CMB. The choice of underlying (basement) unit had little influence on the palaeo-heat flow here calculated as the model was calibrated only for the Stephanian strata. The lithology and stratigraphical thickness of the individual Stephanian formations were taken from Wagner (1971). Following sedimentation of the Stephanian succession there was a long non-depositional duration with periodic erosion up until the Cretaceous. During the Albian to Santonian, diachronous sedimentation of 150–500 m thickness occurred (Vozmediano/Utrillas Formation). Evers (1967) estimated these transgressive sandstones and conglomerates to exceed 500–1,000 m in the area. Following the Alpine orogeny, which led to complex folding and reactivation of Variscan faults along the southern border of the Cantabrian Zone (Alonso et al. 1995), erosion dominated and still persists today.

## Results and interpretation

### Petrographical description of the coaly material

Most coal seam samples and the DOM show signs of weathering at all grades of maturation. Oxidation is focused along cracks and fissures within the coaly particles, giving a darker appearance compared to non-oxidised parts (Fig. 2A). In order to avoid the strong variation caused by oxidation, only the non-oxidised cores of particles were used for measurement in this study. As subjective discrimination criteria the optical appearance was applied. Framboids of pyrite, probably of bacterial origin (Casagrande 1987), are omnipresent both in the coal and in the clastic sediments containing DOM (Fig. 2B). Syngenetic or early-diagenetic growth is evident by the mainly bedding-parallel arrangement of the framboids. The amount of mineral matter associated with the coal particles varies extremely (Fig. 2B) and hindered good quality polishing of the sample material. The DOM can be subdivided into two characteristic groups: I.) cumulation of particles clustered along the bedding plane and oriented with their long axes parallel to

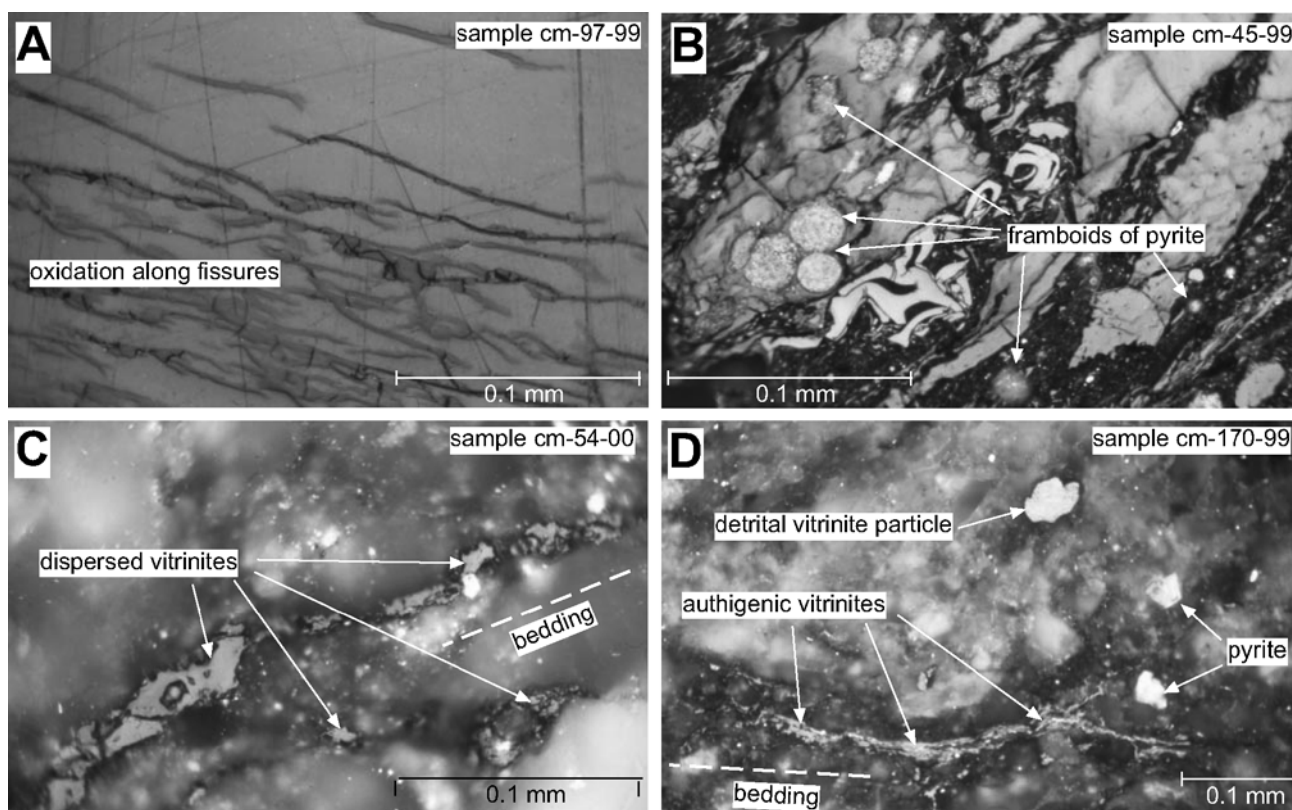


**Fig. 2** Photomicrographs (reflected non-polarised light and oil immersion) showing (A) a vitrinite particle with dark oxidation rims restricted to fissures and small fractures, (B) framboids of pyrite of different sizes in mineral matrix (*darker parts*) and organic matter (*grey*), (C) dispersed vitrinite particles in a bedding parallel arrangement indicating an authigenic origin, (D) two

different types of vitrinite particles: authigenic ones in a bedding parallel arrangement and a reworked (detrital) one with a higher reflectance and sub-angular grain shape. The photos A and B were taken from coal preparations; C and D from polished sections of pelitic siltstones containing DOM

**Table 2** Anisotropy of vitrinite reflectance data. The values of the three principal reflectance axes of the anisotropy ellipsoid and their orientations are calculated using the program of Kelker and Langenberg (1997). The arithmetic error (%) of the measurements is based on six readings per sample, P is the anisotropy factor ( $R_{\max}/R_{\min}$ ) and K is the Flinn factor ( $(R_{\max}/R_{\text{int}})-1/(R_{\text{int}}/R_{\min})-1$ ) (Flinn 1962). Prolate shapes of the ellipsoid are printed bold; orientations are given as dip-direction and angle of dip

Sample	% $R_{\max}$	% $R_{\text{int}}$	% $R_{\min}$	Error (%)	P	K	$R_{\max}$	$R_{\text{int}}$	$R_{\min}$
cmb-10-00	2.06	1.59	1.44	8.9	1.43	<b>2.80</b>	119/36	009/24	253/44
cmb-11-00	1.8	1.69	1.4	8.8	1.29	0.32	348/17	078/02	176/73
cmb-57-00	2.2	1.63	1.57	7.3	1.40	<b>8.27</b>	082/37	246/52	346/08
cmb-26-00	1.76	1.41	1.3	6.0	1.35	<b>2.98</b>	332/31	225/27	101/47
cmb-46-00	2	1.88	1.75	10.6	1.14	0.87	282/01	012/29	191/61
cmb-47-00	1.97	1.87	1.69	8.5	1.17	0.54	244/19	153/05	047/70
cmb-54-00	1.56	1.53	1.31	7.9	1.19	0.14	148/84	273/03	004/05
cmb-55-00	1.71	1.61	1.52	8.6	1.13	<b>1.04</b>	269/19	151/54	010/29
cm-156-99	1.8	1.53	1.43	12.2	1.26	<b>2.82</b>	096/57	191/04	284/33
cm-157-99	2.03	1.81	1.5	9.0	1.35	0.60	350/21	097/38	240/45
cm-158-99	1.88	1.76	1.52	10.5	1.24	0.44	310/17	206/39	059/46
cm-170-99	1.6	1.46	1.39	8.9	1.15	<b>1.78</b>	325/69	070/05	162/20
cm-173-99	1.96	1.77	1.64	9.0	1.20	<b>1.34</b>	238/42	137/12	035/46

this plane (Fig. 2C, D), and II.) sub-angular particles embedded isotropically throughout the grain-supported matrix (Fig. 2D). The latter group has a much higher reflectance and is considered to be of reworked (detrital) origin. The reflectance values of these grains were not included into the AVR database.

#### Anisotropy of vitrinite reflectance (AVR)

The calculated AVR ellipsoids from the 13 measured samples are listed in Table 2. All the samples exhibit distinct anisotropies with 11 to 30% difference in magnitudes between the maximum and minimum reflectance. Presentation in an axial ratio plot (Levine and Davis 1989), which is equivalent to the better known Flinn-diagram (Flinn 1962), indicates variation in the shape of the AVR ellipsoids between strongly oblate (pancake-shaped) and prolate (cigar-shaped) geometry with k-values ranging from 0.14 to 8.27 (Fig. 3).

The orientation of the three principal axes of AVR ellipsoids and structural rock fabric elements are presented for two fold structures developed within the deformed basal succession in equal area stereo-nets (Fig. 4). Siltstone samples cmb-46-00 and cmb-47-00 were obtained from the two limbs of an upright and open fold structure of decimetre scale. Both AVR ellipsoids are biaxial negative, but show a weak anisotropy with only slight differences in the magnitudes of their axes. The foliation of the ellipsoid of sample cmb-46-00 is sub-parallel to the bedding and  $R_{\min}$  lies normal to it, implying burial-dominated coalification. The slight deviation of the reflectance foliation to the bedding in sample cmb-47-00 may indicate a slightly different strain history during coalification than on the opposite fold limb. The lineations of both ellipsoids lie sub-parallel to the fold axis and reflect a syn-tectonic development of the AVR as does the biaxial positive shape of the two AVR ellipsoids.

Three siltstone samples from an upright and tighter fold structure of 5 m wavelength are also presented (Fig. 4). Sample cmb-10-00 from the northern limb shows a typical burial-related coalification pattern with the foliation of the AVR ellipsoid running parallel to the

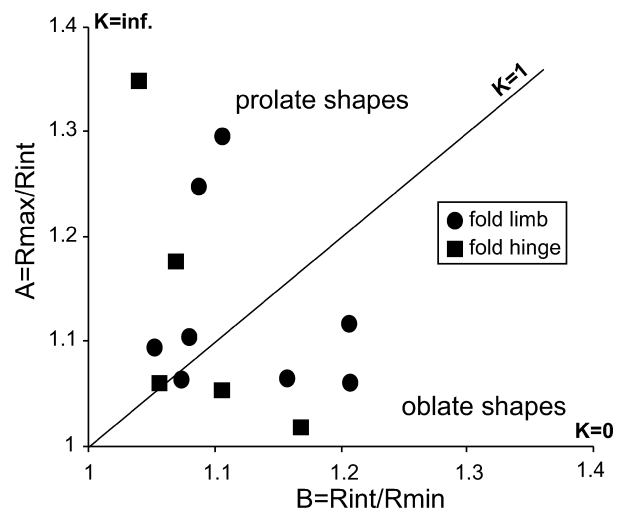


**Fig. 3** Axial ratio plot (Levine and Davis 1989) of principal reflectances used for AVR calculations for samples from the CMB (comparable to the diagram of Flinn 1962). There is a trend from oblate to prolate via intermediate (uniaxial) ellipsoid shapes

bedding and a tectonic increment with the lineation of the ellipsoid parallel to the fold axis. The AVR ellipsoid of sample cmb-11-00 from the southern limb exhibits comparable features to that of sample cmb-47-00 from the open fold structure. Axes' orientations show poor correlation to the fold structure and to the bedding.  $R_{\max}$  and  $R_{\text{int}}$  have approximately the same magnitudes, with no clear lineation definable. This pattern is considered to be typical of burial-related coalification, with no deformational influence, but the ellipsoid foliation lies ca. 40° to the bedding. An explanation for this variance could be lateral gradients induced during deformation. Sample cmb-57-00 collected from the fold hinge shows an approximately uniaxial positive ellipsoid shape, which is quite uncommon in the sample suite. The lineation of the AVR ellipsoid roughly parallels the fold axis, but in contrast to the other two samples from this fold, the foliation of the ellipsoid lies ca. 75° to bedding. In total, there is a trend showing a good parallelism between the lineation of the AVR ellipsoids and fold axes. Within

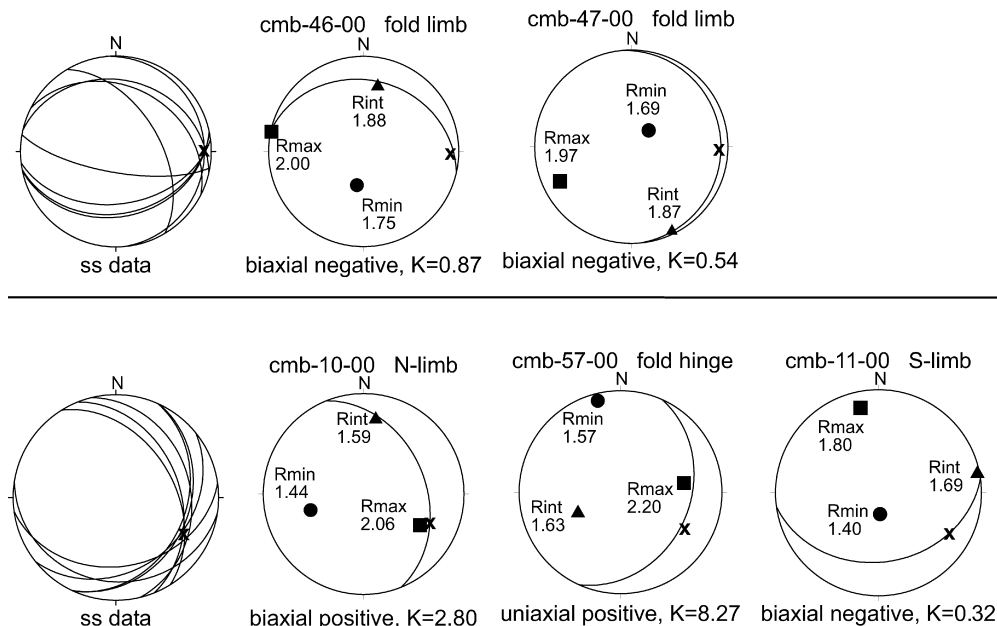


**Fig. 4** Equal area stereo-nets of the orientations of the three principal reflectance axes of AVR ellipsoids for samples from two outcrops. The overall bedding orientations at the sample location are presented by the stereo-nets on the left; the intersections of the great circles correspond to the fold axis (marked by x). The bedding

orientation of the individual samples is shown as a *great circle*, the fold axis by the x. Magnitudes of % vitrinite reflectance are given, also the ellipsoid shape and the Flinn K-factor (Flinn 1962). There is a strong correlation between AVR ellipsoid orientation and geological structure, indicating synchronous development

**Table 3** Results of random vitrinite reflectance measurements (%Rr). The arithmetic error (%) given is calculated from the measured standard deviation. Maximum thicknesses of single formations are also listed. Estimated palaeo-temperatures based on the equations: (1)  $T = (\ln(Rr) + 1.26) / 0.00811$  of Barker and Goldstein (1990); (2)  $T = (\ln(Rr) + 1.68) / 0.0124$  of Barker and Pawlewicz (1994) and (3)  $T = (Rr + 8.6238) / 0.0543$  of Mullis et al. (2001). Reflectance values used in Figs. 5, 6 are printed bold

Sample	Formation	Thickness (m)	%Rr	Error (%)	°C (1)	°C (2)	°C (3)
Cm-35-99	Matallana	300	<b>1.04</b>	3.0	<b>160</b>	<b>138</b>	<b>178</b>
Cm-18-99	Bienvenidas	350–380	0.91	6.3	143	127	175
Cm-131-99	"	"	<b>1.57</b>	4.1	<b>211</b>	<b>172</b>	<b>188</b>
Cmb-52-00	"	"	<b>1.32</b>	2.8	<b>189</b>	<b>158</b>	<b>183</b>
Cm-90-99	San José	75–90	<b>1.42</b>	4.0	<b>199</b>	<b>164</b>	<b>185</b>
Cm-53-99	Roguera	60–70	<b>1.66</b>	2.7	<b>218</b>	<b>176</b>	<b>189</b>
Cm-52-99	Casc.-Rog.	150–170	<b>1.88</b>	3.6	<b>233</b>	<b>187</b>	<b>193</b>
Cm-71-99	"	"	0.76	5.0	121	113	173
Cm-75-99	"	"	<b>1.97</b>	4.9	<b>239</b>	<b>190</b>	<b>195</b>
Cm-43-99	Pastora	85–200	1.43	4.7	199	164	185
Cm-97-99	"	"	1.24	4.2	182	153	182
Cm-146-99	"	"	1.27	6.1	184	154	182
Tm-1-99	"	"	<b>2.03</b>	5.3	<b>243</b>	<b>193</b>	<b>196</b>
Cmb-2-00	"	"	<b>1.59</b>	5.0	<b>213</b>	<b>173</b>	<b>188</b>
Cmb-4-00	"	"	1.36	4.9	194	160	184
Tm-1-00	"	"	<b>2.11</b>	5.6	<b>248</b>	<b>196</b>	<b>198</b>
Tm-2-00	"	"	4.03	4.5	327	248	233
TM-3a-00	"	"	<b>2.56</b>	1.5	<b>271</b>	<b>211</b>	<b>206</b>
TM-3b-00	"	"	<b>2.49</b>	4.8	<b>268</b>	<b>209</b>	<b>205</b>

some samples deviations occur between the foliations of the AVR ellipsoids and the bedding.

#### Mean coalification gradient for the Stephanian strata

Measurements of random vitrinite reflectance (%Rr) were used to evaluate a mean coalification gradient and the total overburden for the CMB, based on the values presented in Table 3. From the 31 samples prepared, only 19 could be measured with certainty. A further seven samples were discarded from the data set because of

intense alteration (retarded reflectance) and close proximity to igneous dykes (elevated reflectance).

To obtain an estimate of the coalification gradient and the total overburden, the method of Yamaji (1986) was applied (see also Conolly 1989; Scheidt and Littke 1989). The %Rr values were plotted on a logarithmic axis due to the observation that in undisturbed settings the increase of %Rr with depth has an exponential form, allowing a linear regression to be calculated from data points (Fig. 5). Assuming that the palaeo-surface vitrinite (huminitic) reflectance was 0.25%Rr (equivalent to palaeo-surface temperature of ca. 25 °C), the intersection

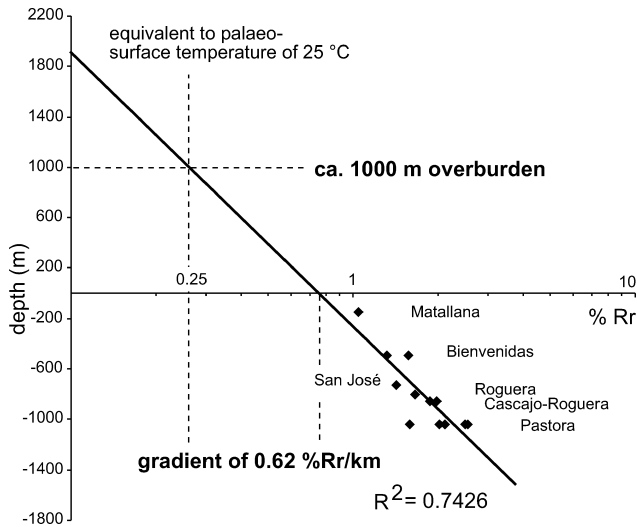


**Fig. 5** Plot of logarithmic %Rr values versus depth used to reconstruct the coalification gradient and the maximum thickness of overburden (Yamaji 1986). The correlation coefficient  $R^2$  of the regression line (*thick line*) indicates a low scattering of the data points and a relatively high quality of the calculated regression. The high coalification gradient of 0.62%Rr/km implies a high thermal palaeo-heat flow

of the regression line at this point can be used to predict the maximum overburden. The %Rr values used for the explained procedure range from 1.04 to 2.56%Rr for the six formations, and produce a coalification gradient of 0.62%Rr/km and a total overburden of about 1,000 m.

#### Mean palaeo-geothermal gradient for the Stephanian strata

The data set of random vitrinite reflectance (%Rr) was also used to calculate a mean palaeo-geothermal gradient for the Stephanian strata by adopting the empirical equations of (1)  $T = (\ln(\%Rr) + 1.26) / 0.00811$  of Barker and Goldstein (1990), (2)  $T = (\ln(\%Rr) + 1.68) / 0.0124$  of Barker and Pawlewicz (1994) and (3)  $T = (\%Rr + 8.6238) / 0.0543$  of Mullis et al. (2001). The results are plotted against depth and the temperature gradient calculated (Fig. 6). Applying the same procedure as in Fig. 5, it is also possible to estimate the total thickness of overburden. According to Eqn. (1) the overburden was about 730 m and the mean palaeo-geothermal gradient about 135 °C/km (Fig. 6A). According to this model the calculated maximum temperature for the lowermost formation (San Francisco) was between 295 and 315 °C. Equation (2) results in a total overburden of 1,020 m and a mean palaeo-geothermal gradient of 85 °C/km (Fig. 6B). The overburden corresponds well with that of Fig. 5, where the measured (true) reflectance values are plotted. Again, the mean temperature gradient is very high but may be viewed as realistic in respect to the abundance of intrusions. Here, the maximum temperature of the lowermost San Francisco Formation would have reached

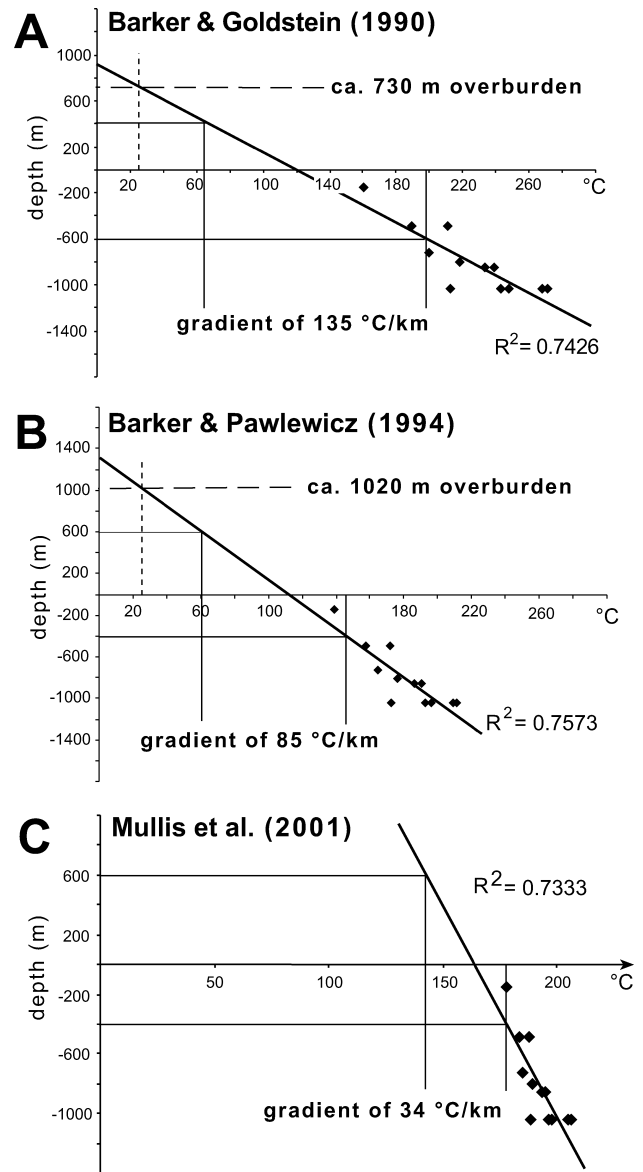


**Fig. 6 A-C** Different models used to reconstruct the maximum overburden and the mean palaeo-geothermal gradient. The models are based on different equations (references are given in text) to calculate temperatures from %Rr values. The correlation coefficient  $R^2$  of the regression lines (*thick lines*) is similar to that in Fig. 5, due to the same source of data

225–240 °C. According to Eqn. (3) the mean palaeo-geothermal gradient was about 34 °C/km and a total overburden in the range of 4,000 m (Fig. 6C). These values appear rather unrealistic considering the presence of magmatic bodies and the lack of geological evidence for such a thick overburden.

#### Palaeo-heat flow and burial history

To obtain a good fit between measured and calculated %Rr values, different scenarios were calculated. The time



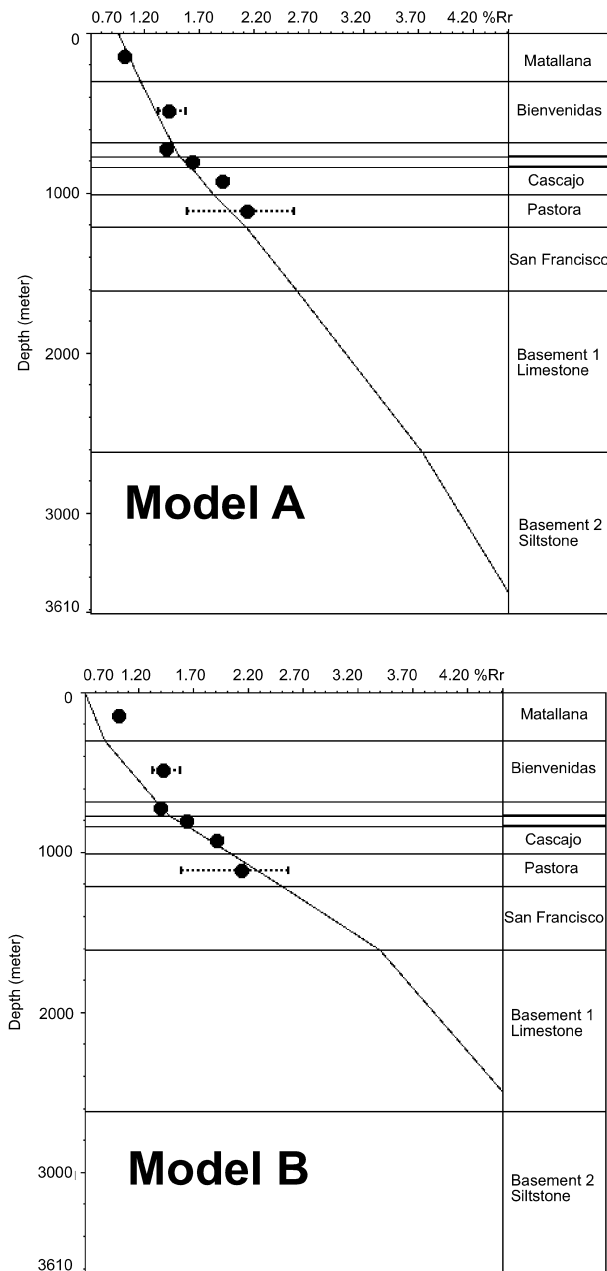


**Fig. 7** Measured (*dots*) and calculated (*line*) vitrinite reflectances for the pseudo-well, reconstructed from outcrop samples. Vitrinite reflectance was calculated using the EASY %Ro method of Sweeney and Burnham (1990). The better calibration fit of Model A was achieved with a palaeo-heat flow of 90 mW/m<sup>2</sup> and an overburden of 2,000 m. The fit of Model B was achieved with a palaeo-heat flow of 150 mW/m<sup>2</sup> and an overburden of 1,050 m. The measured vitrinite reflectance for the two uppermost Stephanian formations (Matallana and Bienvenidas) do not correspond well, but the overburden value is much more likely and fits well with the gradient calculations (Figs. 5 and 6)

of maximum burial was placed in the post-Stephanian, assuming deposition of sedimentary rocks until the end of the Permian and subsequent erosion (Table 1). A good calibration fit was achieved using a palaeo-heat flow of 90 mW/m<sup>2</sup> for the time of maximum burial and a total

overburden of 2,000 m (Fig. 7A). According to this model, maximum temperatures for the Stephanian formations ranged between 185 and 200 °C (top and bottom of San Francisco Formation, respectively). The thicker overburden contrasts with that determined by the methods of Yamaji (1986), Barker and Goldstein (1990) and Barker and Pawlewicz (1994) (Figs. 5 and 6). Therefore a second model (Model B) was calculated assuming an overburden of 1,050 m, as determined by the empirical methods presented. To achieve a good calibration fit, a heat flow of 150 mW/m<sup>2</sup> was adopted for the time of maximum burial. Maximum temperatures for the Stephanian San Francisco Formation range here between 215 and 270 °C. The resulting calibration curve fits the measured %Rr values of the lower Stephanian formations, but deviates strongly from stratigraphically the upper values (Fig. 7B).

The resulting burial history indicates rapid subsidence occurred during Stephanian B to Permian times, followed by high erosion rates (Fig. 8). Heward (1978) estimated a subsidence rate of 0.21–0.36 m/1,000 a for the Stephanian B succession, which is in reasonable agreement with our calculation of 0.23 m/1,000 a. As the age of overburden (1,050 m) cannot be exactly specified, these sediments were not included in the calculation of the subsidence rate. Such calculations are only estimates based on the applied modelling technique. If, for example, it is assumed that all formations were sedimented during the Stephanian B (duration of 2–3 Ma), the subsidence rate was significantly higher, at about 0.5–0.8 m/1,000 a.

## Discussion

### Timing of coalification

In burial sequences an uniaxial oblate AVR ellipsoid geometry is expected for the compaction related anisotropy, with the short axis ( $R_{\min}$ ) lying parallel to the direction of compaction and the long axes ( $R_{\max}$  and  $R_{\text{int}}$ ) parallel to bedding (e.g. Teichmüller 1987a; Gibling et al. 2002). During rock deformation this geometry is modified in respect to the effective deviatoric stresses, whereby the direction of minimum reflectance aligns parallel to the direction of maximum compressional stresses. In folded sequences the maximum reflectance develops in the direction of the fold axis (Levine and Davis 1984; Langenberg and Kalkreuth 1991a, Langenberg et al. 1998). These relationships lead to a general correspondence between the orientation of AVR principale axes and the fabric elements of sedimentary rocks, where  $R_{\max}$  and  $R_{\text{int}}$  are oriented within and  $R_{\min}$  is normal to the bedding plane. This geometry is observed in most of the samples in the CMB. Some samples (e.g. cmb-57-00), however, show notable deviations of the AVR foliation from the orientation of the bedding plane.

The arrangement of the principal AVR axes are considered to reflect a transition state between pre- and syn-deformational influences on the coalification. The

**Fig. 8** 1D numerical modelling of the burial history of the CMB. Input data is shown in Table 1. For calibration of Model B an overburden of 1,050 m was selected (Fig. 7). For further explanation see text

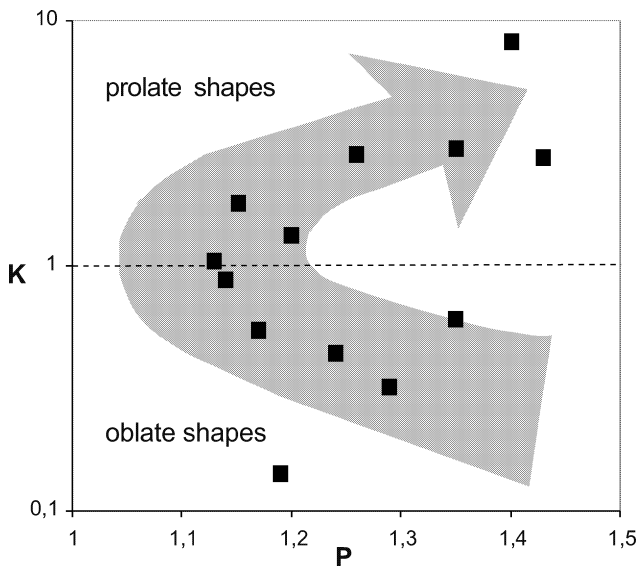
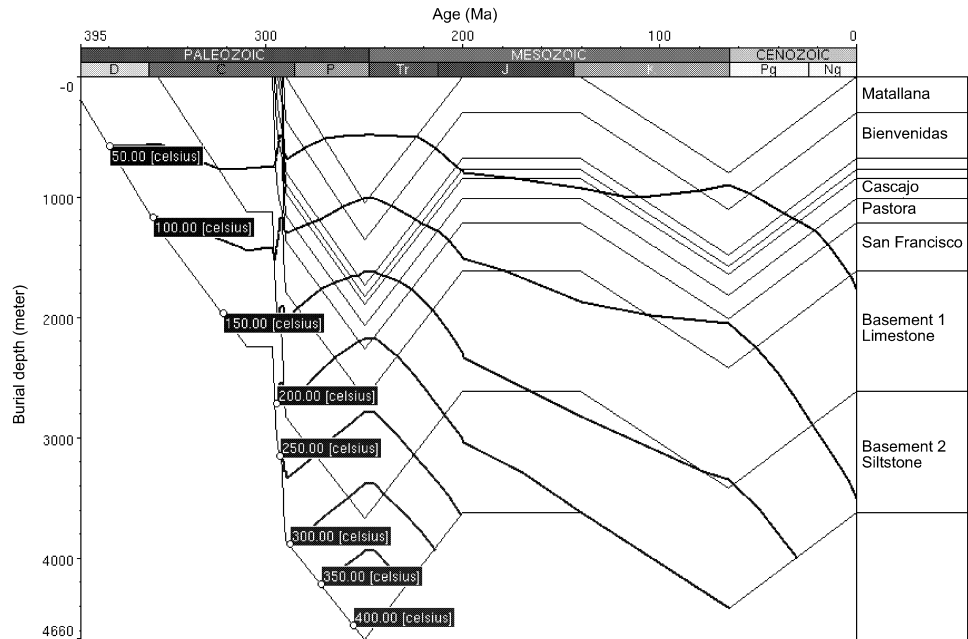


**Fig. 9** Diagram showing the relationship between the shape of AVR ellipsoids and the maximum anisotropy P. Evidently, the path from oblate to prolate geometry is accompanied by a reduction in total anisotropy

fact that most foliations of the AVR ellipsoids run parallel to the bedding whereas  $R_{min}$  is normal to it supports a mainly burial-dominated coalification origin. However, the biaxial character of most of the measured samples, with the ellipsoid lineation ( $R_{max}$ ) running parallel to fold axes, is taken as an indication for a tectonic influence on the development of the AVR. The phenomena of biaxial shapes on fold limbs and a uniaxial shape in fold hinges is also described by Langenberg and Kalkreuth (1991a) for samples from the Cadomin area, Canada, and by Salih and Lisle (1988) for samples from South Wales, UK. It is

assumed that the bulk geometry of the AVR ellipsoids is distinctly oblate due to compaction before modification by tectonic stresses. During a deformation path related to the development of fold structures, regimes of flattening with plane strain and constriction for individual increments and individual geometrical positions may produce AVR ellipsoids of various shapes simultaneously. Folding produces an uniaxial oblate ellipsoid with the minimum axis normal to the fold axial plane. In upright folding (our sample locations), the axial plane will be normal to pre-folding bedding and thus the minimum axis of the folding ellipsoid will be perpendicular to the minimum axis of the compaction ellipsoid. Superposition of the two ellipsoids produces variously shaped, but usually prolate ellipsoids whose major axis lies parallel to the fold axis. However, our analysis of different fold structures shows a distinct trend in the shape of AVR ellipsoids. Fig. 9 presents the ellipsoid shapes versus their maximum anisotropy ( $P = R_{max}/R_{min}$ ). Evidently the path from oblate to prolate geometry is accompanied by a reduction in total anisotropy when the oblate ellipsoid shape is transformed into a triaxial geometry with minimum values at  $k=1$  (plane strain). The anisotropy progressively increases again when transformed into a prolate geometry. The analysed samples from the CMB show a development in their shape and anisotropy as would be predicted during continuous ellipsoid modification from oblate to prolate geometry. The modification of the shape of AVR ellipsoids is therefore interpreted as a result of strain during folding of the CMB rocks.

There is ongoing discussion concerning the influence of Variscan versus Alpine deformation on the tectonic structures at the southern border of the Cantabrian Zone and especially in the CMB (Villegas 1996). The orientation of the inner aromatic structure of the vitrinite

particles is genetically and only linked to the maximum coalification process (Rouzaud and Oberlin 1983; Levine and Davis 1984). Because peak coalification in the CMB was directly related to the late-Variscan intrusion activity, the development of the tectonic increment of the measured AVR must have taken place contemporaneously. A late-Variscan age (Saalic phase) of the major structures of the CMB has already been suggested by Wagner and Artieda (1970) and de Sitter (1965), despite the more recent study of Villegas (1996), who favoured an Alpine age. There is little discussion about the wide extent of Alpine structures along the southern border of the Cantabrian Zone, which is manifested, for example, by the partly overturned Cretaceous and Tertiary sediments along the Sabero-Gordón line (Alonso et al. 1995). However, despite this overturning, our new results demonstrate that the development of the main structures within the CMB occurred during late-Variscan times (Stephanian to Permian). Nevertheless, the lack of parallelism between AVR ellipsoid and structural fabric in some samples may be an expression of Alpine deformational influences. Especially the minor variations of the lineation of some AVR ellipsoids in respect to the fold axes (Fig. 4) could express more than the aforementioned measurement error. These variations could be due to some post-Variscan, maybe Alpine aged fold re-orientation. But it remains unclear why some samples were affected by this re-orientation whereas some others from the same fold structure were obviously not. At least we favour a more likely explanation that relates the observed variations to the characteristic pull-apart setting where maximum coalification and transpressional/transensional deformation were contemporaneous.

Theoretically there is also the possibility of re-orientation of a pre-existing pattern of the aromatic lamellae resulting by physical rotation (Levine and Davis 1989). As this process is not convincingly described yet, especially if there is a need of another coalification event of same magnitude as before or not, we reject it here. On the other hand the discussion clearly shows that further studies are necessary to constrain these relationships, especially the processes, which are responsible for the development of the AVR (see also Gibling et al. 2002). Emphasis should also be given to a direct comparison between AVR ellipsoids and strain analysis in progressive deformed sedimentary rocks.

### Thermal history

An important prerequisite for calculating thermal gradients in sedimentary basins is that the isorefectance lines run parallel or at least sub-parallel to bedding. The validity of our calculations is strongly supported by the good correlation coefficients  $R^2$  (between 0.74 and 0.76) of the regression lines (Figs. 5 and 6), indicating peak coalification to have been more or less contemporaneous with peak burial. The scatter of %R values within each formation is probably more dependent on two other

factors, such as contact effects of magmatic bodies and weathering. In this study it was not possible to discriminate between and eliminate these two factors. The chosen procedure to construct the pseudo-well (mean lithostratigraphical thickness for each formation) reduces the influence of the scattering. Due to the complex tectonic structure of the CMB and significant lateral changes in thickness of the several Stephanian formations, this procedure appears to be the most realistic approach. Additional support for the validity of our calculations are the AVR ellipsoid foliations, which are oriented mainly parallel to the bedding whereas  $R_{\min}$  lies normal to it, indicating a strong burial influence during coalification. The fact that the AVR shows a tectonic influence during coalification is of no relevance for the thermal calculations, because there was no increase in coal rank combined with the development of the AVR.

In sedimentary basins the increase in vitrinite reflectance and the resulting rank of the organic matter is generally considered to be dependent on burial depth, time and the related palaeo-thermal history. The two most important factors are considered to be the palaeo-geothermal gradient and the palaeo-heat flow (Welte et al. 1997; Taylor et al. 1998). In this study, the mean palaeo-geothermal gradient calculations and palaeo-heat flow modelling are based on the assumption that the maximum coalification reflects peak burial and peak temperature conditions, which in turn are directly related to the magmatic activities of late-Variscan age. Mendez (1985) already stated that the intrusion activities exerted most influence on the overall coalification grade with locally restricted anomalies at direct contacts to the magmatic material.

Applying these assumptions the validity of the different empirical equations used for calculation of the different gradients can be evaluated. As the reconstructed overburden of 1,000 m of Fig. 5 is based on measured reflectance values, we regard this as a reliable reference value against which thermal calculations can be compared. The most unrealistic values are clearly those derived from Eqn. (3) of Mullis et al. (2001) (Fig. 6C), based on the comparison of vitrinite data with homogenisation temperatures of fluid inclusions in syn-kinematically grown fibre quartz. The coalification process in the CMB is notably inconsistent with the fluid inclusion data, and it therefore appears that this equation is only valid for the Alpine study area of Mullis et al. (2001). It is evident that such correlations must be treated with caution, especially if no structural or timing constraints are available. Equation (1) of Barker and Goldstein (1990) appears to provide a more realistic estimate for the CMB, despite the fact that the conversion is also based on the comparison with homogenisation temperatures of fluid inclusions from re-equilibrated calcite, and additionally to present-day peak borehole temperatures. These authors concluded that %Rr is most closely related to peak temperature than to the duration of heating. A mean palaeo-geothermal gradient of 135 °C/km for the CMB (Fig. 6A) indicates a strong influence of the magmatic

intrusions on the coalification. However, the calculated maximum temperature of 295 to 315 °C for the lowermost San Francisco Formation distinctly exceeds the upper temperature limit predicted from illite crystallinity data (Frings 2002). Overall, it appears that Eqn. (3) neglects the influence of intrusive activity on the coalification, whereas Eqn. (1) overestimates it.

The most realistic results are obtained by applying Eqn. (2) of Barker and Pawlewicz (1994). This equation is based on comparisons between vitrinite reflectance and present-day borehole temperatures. The authors concluded that the maximum temperature or effective heating time (time within 15 °C of maximum temperature) is the most important factor on coalification. They also stated that the functional heating duration is negligible above 10,000 years to more than 10 Ma. The reconstructed overburden of 1,020 m is in accordance with that calculated directly from the vitrinite reflectance data (Fig. 5). The elevated mean palaeo-geothermal gradient of 85 °C/km correlates well with the high coalification gradient of 0.62 %Rr/km, and both indicate a significant influence from magmatic activity. The maximum temperature of 225–240 °C predicted for the lowermost San Francisco Formation is in the range of the temperature indicated by illite crystallinity results (Frings 2002) and coincides with the gradients given by Mendez (1985) and Galan et al. (1978).

Sachsenhofer and Littke (1992) showed that the approach of Barker and Pawlewicz (1986), which is quite similar to that of Barker and Pawlewicz (1994), yields only good results in the case of short and simple thermal histories. According to Sachsenhofer and Littke (1992) the calculated temperatures in areas of occasionally high palaeo-heat flow with some magmatic activity are often too high in the low-temperature range and too low in the high-temperature range. Compared to results obtained with the kinetic approach of EASY %Ro (Sweeney and Burnham 1990), they rejected the approach of Barker and Pawlewicz (1986) as being too inaccurate when dealing with complex thermal histories. We agree that the various equations are applicable only to specific settings of particular thermal histories, as shown by our own results. However, as the calculated value for the overburden is in accordance with that yielded with the approach of Yamaji (1986), the calculated mean palaeo-geothermal gradient is seen to provide a good estimate of the real palaeo-thermal history of the CMB. Nevertheless, we used the kinetic EASY %Ro approach for calibration of the 1D modelling and obtained some reliable models (Model B) in the range of the empirical results.

From the available calibration data two numerical 1D models were established. In Model A, a heat flow of 90 mW/m<sup>2</sup> was assumed for the time of maximum burial with a total overburden of 2,000 m. These assumptions produced a good fit between measured and calculated vitrinite reflectance values (Fig. 7A). In Model B, a heat flow of 150 mW/m<sup>2</sup> was adopted and a total overburden of 1,050 m. This model also produced a good fit with the measured values at greater depth but not for the

Bienvenidas and Matallana Formations (Fig. 7B). Generally, the Barker and Pawlewicz (1994) method agrees well with the EASY %Ro algorithm if the heating time was sufficiently long (~5 Ma) (Büker 2002). If the data points of the Bienvenidas and Matallana Formations are discarded, an overburden of about 1,000 m can be simulated from the numerical modelling (Fig. 8). Heat flows of about 150 mW/m<sup>2</sup>, as assumed in our Model B, are generally related to active ocean ridges and volcanoes (Allen and Allen 1990). More appropriate seems to be the most recent model explaining the widespread magmatism at late-Variscan times in the Cantabrian Zone, which relates this phenomena to delamination of the crust and upwelling of the asthenosphere (Fernandez-Suarez 1998; Fernandez-Suarez et al. 2000). Additionally palaeo-heat flows in the range of Model B are reported from similar settings such as the Eastern Alps (Sachsenhofer 2001).

The overburden estimate of approximately 1,000 m is in rough accordance with the estimated thickness of Cretaceous transgressive sediments (Evers 1967). It is, however, unlikely that this Cretaceous cover has had any significant influence on the coalification of the organic material of the CMB. As the estimates of this study deal only with overburden relevant to the coalification process, it is more likely that peak temperatures and maximum burial were attained much earlier than Cretaceous times and are related to the intrusive activities of late-Variscan age. Therefore it is considered more probable that the overburden relates to further sedimentation in Stephanian or even lower Permian times. This scenario is supported by several studies (Comte 1959; de Sitter 1962; van Ameron and van Dillewijn 1963; Heward 1978; Martinez-Garcia and Wagner 1984), which describe the Stephanian palaeo-depositional environment in the area of the CMB as a large, coherent coastal floodplain with alluvial fan and lacustrine sedimentation, with depocenters/deep depressions forming along major structural lineaments, such as the Sabero-Gordón line. Such sediments have been subsequently affected by tectonic deformation and eroded, whereby only the Stephanian sequences of the former depocenters have been preserved. Martinez-García (1990) also predicted a Permian cover to have overlain the whole Cantabrian Zone. But it is considered unlikely that such a cover exceeded 1,000 m thickness in the CMB, as only very small outcrops of Permian strata are preserved in the north of the Cantabrian Zone. At present there is no direct way to constrain the thickness of overburden based on sedimentological or structural data (e.g. palinspastic reconstructions). On the basis of our palaeo-geothermal results it is most likely that the reconstructed overburden reflects eroded Stephanian to Permian strata, as it is shown in Fig. 8 and Table 1.

The presented study combines investigations of the coalification pattern (thermal history) with the rock deformation. Although the CMB is characterised by complex pull-apart tectonics our approach allows us to reconstruct the tectono-thermal history with greatest accuracy. The AVR is tested as a reliable tool to achieve this correlation. Some of the variations between fold

structures and AVR ellipsoids may be influenced by later (Alpine) events, but the main deformation was definitely contemporaneous with peak coalification at late-Variscan times. The reconstruction of the thermal history is achieved best with the empirical equation of Barker and Pawlewicz (1994). It seems that most of the critics of Sachsenhofer and Littke (1992) are not applicable to the pull-apart setting of the CMB. Thermal modelling with the favoured EASY %Ro method results a good fit (Model A), but with minor geological relevance. Only with additional information about the basin history the more realistic Model B could be developed. It has to be mentioned that we disregarded the influence of fluids in our modelling and discussion. It is possible that there were more complexity and processes active than mentioned, and some of the observed variations might be due to thermal fluid-induced parameters (Hower and Gayer 2002).

## Conclusions

1. The AVR data indicates a transition state between a pre- and a syn-deformational coalification pattern. Burial related coalification produced AVR shapes with ellipsoid foliation mainly running sub-parallel and  $R_{\min}$  ellipsoid axes normal to bedding, modified by a significant syn-deformational influence of tectonic strain as indicated by biaxial positive shapes and AVR ellipsoid lineations ( $R_{\max}$  ellipsoid axis) running parallel to fold axes. The modification from an oblate to prolate geometry of the AVR ellipsoid shapes is interpreted as a result of strain during folding of the CMB.
2. Coalification of organic material in the CMB was influenced by a high mean palaeo-geothermal gradient of ca. 85 °C/km, which resulted in a mean coalification gradient of 0.62%Ro/km for the Stephanian strata. Local anomalies, related to intrusion "aureoles", show an enhanced coalification grade of the organic material, whereas mostly all samples exhibit varying levels of alteration (oxidation).
3. According to the calculated gradients the total overburden relevant to the maximum coalification is estimated to be in the order of 1,000 m. This overburden is attributed to overlying Stephanian to Permian rocks that have subsequently been eroded.
4. Numerical 1D-modelling of palaeo-heat flow resulted in two models, one with an assumed heat flow of 90 mW/m<sup>2</sup> and an overburden of 2,000 m (Model A) and another preferred one with a heat flow of 150 mW/m<sup>2</sup> and an overburden of 1,050 m (Model B).
5. For the thermal description of a complex pull-apart setting the applied combination of empirical equations, thermal modelling and AVR measurement proved a reliable approach.

**Acknowledgements** This work was funded by the Deutsche Forschungsgemeinschaft (DFG-grant WA 10/10 2-1 and 2-2) and forms part of the doctoral thesis of the principal author. S.A. Hullera Vasco-Leonesa (Spain) is thanked for the permission to visit the open pit at Santa Lucia and the underground mine of Tabliza. O. Wallerath (Heidelberg) is thanked for preparing and polishing the very difficult material. R. Littke (Aachen, Germany) is thanked for kindly allowing us to measure some samples at the Lehrstuhl für Geologie, Geochemie und Lagerstätten des Erdöls und der Kohle in Aachen. Detailed reviews of an earlier version of the manuscript by W. Kalkreuth (Porto Alegre, Brasil) and R. Littke improved the quality of the text and are gratefully acknowledged. W. Langenberg (Edmonton, Canada) is thanked for permission to use his AVR calculation program. The constructive reviews of R. Gayer and J. Hower are also gratefully acknowledged.

## References

- Allen PA, Allen JR (1990) Basin analysis: principles and applications. Blackwell, Oxford, pp 1-451
- Alonso JL, Pulgar JA, García Ramos JC, Barba P (1995) Tertiary basins and alpine tectonics in the Cantabrian Mountains (NW Spain). In: Friend PF, Dabrio CJ (eds) Tertiary basins of Spain. Cambridge University Press, pp 214-227
- Amerom van HWJ, Dillewijn van J (1963) Note sur le bassin houllier de Ciñera-Matallana. Leidse Geol Mededelingen 29:303-312
- Barker CE, Goldstein RH (1990) Fluid-inclusion technique for determining maximum temperature in calcite and its comparison to the vitrinite reflectance geothermometer. *Geology* 18:1003-1006
- Barker CE, Pawlewicz MJ (1986) The correlation of vitrinite reflectance with maximum temperature in humic organic matter. In: Buntebarth G, Stegena L (eds) Palaeogeothermics. Springer, Berlin Heidelberg New York, pp 79-93
- Barker CE, Pawlewicz MJ (1994) Calculation of vitrinite reflectance from thermal histories and peak temperatures. A comparison of methods. In: Mukhopadhyay PK, Dow WG (eds) Vitrinite reflectance as a maturity parameter: applications and limitations. ACS Symp Series 570:216-229
- Bieg G, Burger K (1992) Preliminary study of tonsteins of the Pastora Formation (Stephanian B) of the Ciñera-Matallana Coalfield, northwestern Spain. *Int J Coal Geol* 21:139-160
- Büker C (2002) Paläotemperaturindikatoren und ihre geologische Interpretation. [Online]. Available from World Wide Web: <http://www.rwth-aachen.de/lek/Ww/CBPalaeotemp.html> [Cited 2002-10-18]
- Casagrande DJ (1987) Sulphur in peat and coal. In: Scott AC (ed) Coal and coal-bearing strata. *Geol Soc Lond Spec Publ* 32:87-106
- Comte P (1959) Recherches sur les terrains anciens de la Cordilliere Cantabrique. *Memorias Inst Geol Min Espana* 60:1-440
- Connolly CA (1989) Thermal history and diagenesis of the Wilrich Member shale, Spirit River Formation, northwest Alberta. *Can Petrol Geol Bull* 37:182-197
- Evers HJ (1967) Geology of the Leonides between the Bernesga and Porma rivers, Cantabrian Mountains, NW Spain. *Leidse Geol Mededelingen* 44:83-151
- Fernandez-Suarez J (1998) Granitoid magmatism in the autochthonous of the NW Iberian Variscan belt: an overview. In: Arias D, Martin-Izard A, Paniagua A (eds) Gold: exploration and mining in NW Spain. Intern. meeting, Oviedo, pp 12-19
- Fernandez-Suarez J, Dunning GR, Jenner GA, Gutierrez-Alonso G (2000) Variscan collisional magmatism and deformation in NW Iberia: constraints from U-Pb geochronology of granitoids. *J Geol Soc* 157:565-576
- Flinn D (1962) On folding during three-dimensional progressive deformation. *Quat J Geol Soc Lond* 118:385-433

- Frings KH (2002) Paläotemperatur-Anomalien in spätvariskischen Kohlebecken am Beispiel des Ciñera-Matallana Beckens, Kantabrisches Gebirge, NW Spanien. *Geol-Pal Inst Univ Heidelberg Germany, Gaea heidelbergensis* 11:1–136
- Galan E, Aparicio A, Villegas HFJ (1978) El metamorfismo de muy bajo grado (anquimetamorfismo) de la cuenca carbonifera Ciñera-Matallana (Provincia de Leon). *Estud Geol* 34:505–510
- García-Lopez S, Bastida F, Brime C, Aller J, Valin ML, Sanz-Lopez J, Mendez CA, Menendez-Alvarez JR (1999) Los episodios metamorficos de la Zona Cantabrica y su contexto estructural. *Trab Geol* 21:177–187
- Gibling MR, Langenberg W, Kalkreuth WD, Waldron JWF, Courtney R, Paul J, Grist AM (2002) Deformation of Upper Carboniferous coal measures in the Sydney Basin: evidence for late Alleghanian tectonism in Atlantic Canada. *Can J Earth Sci* 39:79–93
- Hertle M, Littke R (2000) Coalification pattern and thermal modelling of the Permo-Carboniferous Saar Basin (SW Germany). *Int J Coal Geol* 42:273–296
- Heward AP (1978) Alluvial fan and lacustrine sediments from the Stephanian A and B (La Magdalena, Cinera-Matallana and Sabero) coalfields, northern Spain. *Sedimentology* 25:451–488
- Heward AP, Reading HG (1980) Deposits associated with a Hercynian to late Hercynian continental strike-slip system, Cantabrian Mountains, Northern Spain. *Spec Publ Assoc Sediment* 4:105–125
- Hirsch PB (1954) X-ray scattering from coals. *Proc R Soc Lond Ser A, Math Phys Sci* 226, 1165:143–169
- Hower JC, Davis A (1981a) Application of vitrinite reflectance anisotropy in the evaluation of coal metamorphism. *Geol Soc Am Bull* 92/1:350–366
- Hower JC, Davis A (1981b) Vitrinite reflectance anisotropy as a tectonic fabric element. *Geol* 9:165–168
- Hower JC, Gayer RA (2002) Mechanisms of coal metamorphism: case studies from Paleozoic coalfields. *Int J Coal Geol* 50:215–245
- Julivert M (1971) Decollement tectonics in the Hercynian Cordillera of NW Spain. *Am J Sci* 270/1:1–29
- Kalkreuth W, Langenberg W, McMechan M (1989) Regional coalification pattern of Lower Cretaceous coal-bearing strata, Rocky Mountain Foothills and foreland, Canada – implications for future exploration. *Int J Coal Geol* 13:261–302
- Karweil J (1956) Die Metamorphose der Kohlen vom Standpunkt der physikalischen Chemie. *Z Dtsch Geol Ges* 107:132–139
- Kelker D, Langenberg W (1997) Ellipsoid estimation in coal reflectance anisotropy. *Math Geol* 29/2:185–198
- Krumm S (1992) Illitkristallinität als Indikator schwacher Metamorphose – Methodische Untersuchungen, regionale Anwendungen und Vergleiche mit anderen Parametern. *Erlanger Geol Abh* 120:1–75
- Langenberg W, Kalkreuth W (1991a) Reflectance anisotropy and syn-deformational coalification of the Jewel seam in the Cadomin area, Alberta, Canada. *Int J Coal Geol* 19:303–317
- Langenberg W, Kalkreuth W (1991b) Tectonic controls on regional coalification and vitrinite-reflectance anisotropy of Lower Cretaceous coals in the Alberta Foothills, Canada. *Soc Géol France Bull* 162/2:375–383
- Langenberg W, Kalkreuth W, Holmes K (1998) Components of syn- and post-deformational coalification in the Mountain Park area, west central Alberta. *Petrol Geol Can Bull* 46/4:564–575
- Levine JR, Davis A (1984) Optical anisotropy of coals as an indicator of tectonic deformation, Broad Top Coal Field, Pennsylvania. *Geol Soc Am Bull* 95:100–108
- Levine JR, Davis A (1989) The relationship of coal optical fabrics to Alleghanian tectonic deformation in the central Appalachian fold-and-thrust belt, Pennsylvania. *Geol Soc Am Bull* 101:1333–1347
- Lopatin NV (1971) Temperature and geologic time as factors in coalification. *Akad Nauk SSSR, Ser Geol Izvestiya* 3 (Translation from Russian by N. Bostick). pp 95–106
- Lotze F (1945) Zur Gliederung der Iberischen Meseta. *Geotekton Forschungshfte* 6:78–92
- Marschik R (1992) Der Übergang von der Diagenese zur sehr niedriggradigen Metamorphose im externen Varistikum (Kantabrische Zone), NW Spanien. Unpubl Diploma Thesis, Univ Heidelberg Germany, pp 1–70
- Martinez-Garcia E (1990) Stephanian and Permian basins. In: Dallmeyer RD, Martinez-Garcia E (eds) *Pre-Mesozoic geology of Iberia*. Springer, Berlin Heidelberg New York, pp 39–54
- Martinez-Garcia E, Wagner RH (1984) The post-Asturian marine basin of late Stephanian age in northwest Spain. In: Belt ES, MacQueen RW (eds) *CR IX Congress International Stratigraphie Geologique Carbonifere*, Washington DC, Champaign/Urbana 1979. Southern Illinois Univ Press, Carbondale, Edwardsville 3:508–516
- Mendez-Cecilia AF (1985) Estudio de la evolucion de los carbones de la cuenca Cinera-Matallana, Leon. Unpubl PhD Thesis, Univ Oviedo, Spain, pp 1–269
- Merriman RJ, Kemp SJ (1996) Clay minerals and sedimentary basin maturity. *Min Soc Bull* 111:7–8
- Mullis J, Wolf M, Ferreiro-Mählmann R (2001) Temperature determination through fluid inclusion microthermometry and vitrinite reflectance values in the Diagenetic- and Anchi-Zones. *J Conf Abstr (EUG XI, Strassbourg)* 6:230
- Nijman W, Savage JF (1989) Persistent basement wrenching as controlling mechanism of Variscan thin-skinned thrusting and sedimentation, Cantabrian Mountains, Spain. *Tectonophysics* 169:281–302
- Nöth S, Karg H, Littke R (2001) Reconstruction of Late Palaeozoic heat flows and burial histories at the Rhenohercynian-Subvariscan boundary, Germany. *Int J Earth Sci* 90:234–256
- Nöth S, Thomson RO, Littke R (2002) A method for assessing statistical significance and uncertainties for calibration of 1-D thermal basin maturation models. *AAPG Bull* 86/3:417–431
- Oncken O (1982) Zur Rekonstruktion der Geosynklinalgeschichte mit Hilfe von Inkohlungskurven (am Beispiel Ebbeantiklinorium, Rheinisches Schiefergebirge). *Geol Rundsch* 71:579–602
- Rouzaud JN, Oberlin A (1983) Contribution of high-resolution transmission microscopy (TEM) to organic materials characterization and interpretation of their reflectance. In: Durand B (ed) *Thermal phenomena in sedimentary basins*. Editions Technip, Paris, pp 127–134
- Rouzaud JN, Oberlin A (1990) The characterization of coals and cokes by transmission electron microscopy. In: Charcosset H (ed) *Advanced methodologies in coal characterization*. Elsevier, Amsterdam, *Coal Sci Techn* 15:311–355
- Sachsenhofer RF (2001) Syn- and post-collisional heat flow in the Cenozoic Eastern Alps. *Int J Earth Sci* 90:579–592
- Sachsenhofer RF, Littke R (1992) Vergleich und Bewertung verschiedener Methoden zur Berechnung der Vitrinitreflexion am Beispiel von Bohrungen im Steirischen Tertiärbecken. *Zbl Geol Pal* 6:597–610
- Salih MR, Lisle RJ (1988) Optical fabrics and their relation to tectonic deformation at Ffos Las, South Wales Coalfield. *Ann Tectonicae* 2:98–106
- Scheidt G, Littke R (1989) Comparative organic petrology of interlayered sandstones, siltstones, mudstones and coals in the Upper Carboniferous Ruhr basin, northwest Germany, and their thermal history and methane generation. *Geol Rundsch* 78/1:375–390
- Sitter de LU (1962) The structure of the southern slope of the Cantabrian Mountains. Explanation of a geological map with sections (scale 1:100.000). *Leidsche Geol Mededelingen* 26:255–264
- Sitter de LU (1965) Hercynian and Alpine orogenies in northern Spain. *Geol Mijnbouw* 44:373–383
- Stone IJ, Cook AC (1979) The influence of some tectonic structures upon vitrinite reflectance. *J Geol* 87:497–508
- Sweeney JJ, Burnham AK (1990) Evaluation of a simple model of vitrinite reflectance based on chemical kinetics. *AAPG Bull* 74:1559–1570
- Taylor GH, Teichmüller M, Davis A, Diessel CFK, Littke R, Robert P (1998) *Organic petrology*. Gebrüder Borntraeger, Berlin, pp 1–704

- Teichmüller M (1987a) Recent advances in coalification studies and their application to geology. In: Scott AC (ed) *Coal and coal-bearing strata: recent Advances*. Geol Soc Spec Publ 32:127–169
- Teichmüller M (1987b) Organic material and very low-grade metamorphism. In: Frey M (ed) *Low-temperature metamorphism*. Blackie & Son, Glasgow, pp 114–161
- Teichmüller M, Teichmüller R (1966) Geological causes of coalification. *Coal Sci Adv Chem Ser* 55:133–155
- Ting FTC (1981) Uniaxial and biaxial vitrinite reflectance models and their relationship to palaeotectonics. In: Brooks J (ed) *Organic maturation studies and fossil fuel exploration*. Academic Press, London, pp 379–392
- Villegas FJ (1996) Exploracion e investigacion de un nuevo yacimiento de carbon en la cuenca minera Cinera-Matallana (Leon). Unpubl PhD Thesis, Univ Complutense, Madrid, Spain, pp 1–417
- Wagner RH (1971) The stratigraphy and structure of the Cinera-Matallana coalfield (Prov. Leon, N.W. Spain). *Trab Geol* 4:385–429
- Wagner RH, Artieda JI (1970) La cuenca minera Cinera-Matallana. Internal report S.A. Hullera Vasco Leonesa, pp 1–289
- Waples DW (1980) Time and temperature in petroleum formation: application of Lopatin's method to petroleum exploration. *AAPG Bull* 64:916–926
- Welte DH, Horsfield B, Baker DR (1997) *Petroleum and basin evolution*. Springer, Berlin Heidelberg New York, pp 1–535
- Welte DH, Yalcin MN (1988) Basin modelling – a new comprehensive method in petroleum geology. *Org Geochem* 13/1–3:141–151
- Yalcin MN, Littke R, Sachsenhofer RF (1997) Thermal history of sedimentary basins. In: Welte DH, Horsfield B, Baker DR (eds) *Petroleum and basin evolution*. Springer, Berlin Heidelberg New York, pp 71–168
- Yamaji A (1986) Analysis of vitrinite reflectance-burial depth relations in dynamical geological settings by direct integration method. *J Jpn Assoc Petrol Technol* 51/3:1–8